Computational Insights into CO_2-to-Ethane Reduction via a Bioinspired Methyltransferase Molecular Catalyst

João V. F. da Costa[1], Ataualpa A. C. Braga*

[1]*Departamento de Química Fundamental, Universidade de São Paulo, São Paulo, Brazil*
E-mail: ataualpa@iq.usp.br

Abstract

ABSTRACT – While most molecular catalysts reduce CO_2 to single-carbon products (CO, HCOOH, CH_3OH, etc.), few can generate C_2 products like ethane (C_2H_6), a feat typically dominated by heterogeneous systems. Recently, a thiol-functionalized iron porphyrin catalyst achieved CO_2-to-ethane conversion with H_2O as a proton source, reaching ~40% Faradaic efficiency. This study explores the mechanistic pathway, focusing on the critical *first* methyl incorporation onto the pendant thiol (2nd sphere) and subsequent C–C coupling via *second* CO_2 reduction at the metal center. Computational insights reveal how sequential methyl transfers enable ethane formation, bridging bioinspired design with sustainable C_2 synthesis.

Keywords: CO_2 reduction, iron porphyrin, ethane synthesis, methyltranferase

Introduction

Iron porphyrins are well-established electrocatalysts for CO_2 reduction to CO, exhibiting high selectivity, activity, and low overpotentials (1-3). Recent advances have extended their reactivity to CH_4 production via an $8e^-/8H^+$ process (4), while structural modifications (e.g., secondary coordination sphere tuning) can redirect selectivity toward HCOOH (5,6). Typically, CO dominates due to rapid dissociation from the Fe(I)–CO intermediate. However, stabilizing CO binding—e.g., via secondary sphere engineering—enables further reduction. For instance, Dey *et al.* demonstrated that an iron porphyrin with tailored 2nd sphere groups could reduce CO to CH_4 in both aqueous and nonaqueous media (7).

Building on this strategy, the same group recently reported a thiol-modified iron porphyrin that achieves CO_2-to-ethane (C_2H_6) conversion with a remarkable ~40% Faradaic efficiency (8). Experimental evidence suggests a mechanistic sequence: (a) initial CO_2 reduction generates a $–CH_3$ group that binds to the pendant thiol, followed by (b) reduction of a second CO_2 molecule to form a Fe(II)–CH_3 species, enabling C–C coupling between the two methyl groups.

In this work, we employ *Density Functional Theory (DFT)* to elucidate the detailed mechanism of this ethane-forming pathway, focusing on the critical roles of the thiol modifier and sequential methyl transfers.

Experimental

Computational details

Quantum chemical calculations were performed using the Gaussian 16 software package (9) with the B3LYP-D3(BJ) functional (10), which incorporates Grimme's D3 dispersion correction with Becke-Johnson damping (11). Geometry optimizations and frequency calculations were conducted in acetonitrile solvent using the SMD implicit solvation model to account for solvent effects. The def2-SVP (12) basis set was employed to confirm the nature of the structures as minima (no imaginary frequencies), intermediates, or transition states (one imaginary frequency). Intrinsic reaction coordinate (IRC) (13,14) calculations were performed to verify the connectivity between minima and transition states.

For higher accuracy in electronic energies, single-point calculations were carried out in acetonitrile using the larger def2-TZVPP (15) basis set. Redox potentials were calculated by referencing the experimental absolute potential of the standard hydrogen electrode (SHE) in acetonitrile (4.52 V) (16). The B3LYP functional was chosen due to its well-established reliability in modeling iron porphyrin systems (17,18). For clarity, all of the redox potentials reported in this work are relative to SHE in acetonitrile.

Although water is the proton source in Patra *et al.*'s experimental work, theoretical studies suggest that proton transfer from water is both kinetically and thermodynamically unfavorable. Instead, H_2CO_3 (carbonic acid) was considered as the proton donor, as it can form from CO_2 in the presence of residual water. This study focuses on the thermodynamics and kinetics of CO_2 reduction with H_2CO_3 as the proton source (19).

The experimental solubility of CO_2 in acetonitrile under saturated conditions is ~270 mM (20). To account for

standard state corrections, an energy adjustment of –4.0 kcal·mol⁻¹ was applied for carbonic acid (from 1 M to saturated CO_2 conditions). For all other species, a correction of +1.9 kcal·mol⁻¹ was applied.

The Interaction Region Indicator (IRI) analysis (21) was employed to characterize the interactions between the sulfur atom (thiol group) and the carbon atom (methylidene intermediate), providing insights into the electronic structure of the transition state for the S-methyl transfer step. Grid data for the IRI analysis were generated using Multiwfn (version 3.8) (22), and the resulting isosurfaces were visualized with VMD (version 1.9.4) (23).

Results and Discussion

Proposed catalytic cycle and catalyst activation study

Based on experimental results, the catalytic cycle (Fig. 1) begins with the formation of the active Fe(0)-porphyrin species, generated through a multi-electron reduction of the initial $FeTPPC_2SHCl$ catalyst, followed by dissociation of the chloride ligand.

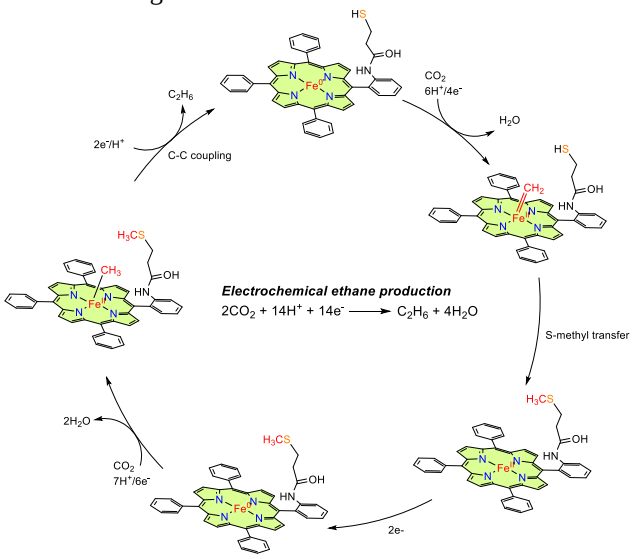

Figure 1. Proposed Mechanism for Reduction of CO_2 to C_2H_6 by Iron Tetraphenylporphyrin complex with thiol pendant based on experimental results in the work of Patra *et al.*

As illustrated in Fig. 2, the initial catalyst, $FeTPPC_2SHCl$ (0), undergoes a one-electron (1e⁻) reduction to form the $[FeTPPC_2SHCl]^-$ (1) intermediate. A second one-electron reduction then generates the $[FeTPPC_2SHCl]^{2-}$ species, which undergoes dissociation of the chloride ligand to yield the active catalyst, $[FeTPPC2SH]^-$.

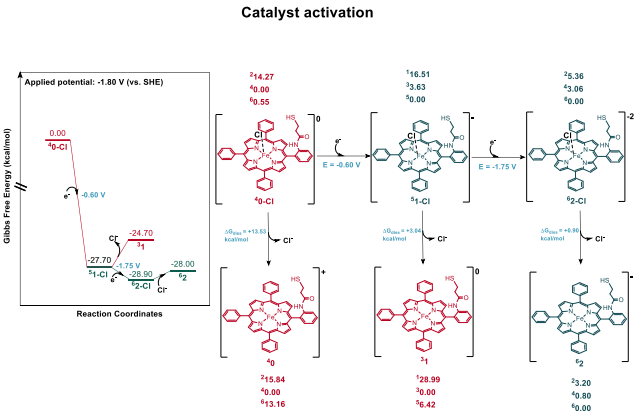

Figure 2. Two one-electron reduction steps and chloride dissociation from the initial catalyst to generate the active species. The number in the left superscript indicates the spin state, followed by the relative energy of each specie in low, intermediate and high-spin multiplicity.

All possible spin-state was calculated for all intermediate in this catalyst activation process. In all intermediate obtained after chloride dissociation, the intermediate-spin species was found to be the ground state. The relative energies and the spin state are shown in Figure 2.

Reduction of CO_2 to methylidene intermediate

The catalytic cycle begins with the one-electron reduction of complex 2 ($[FeTPPC2SH]^-$) to form complex 3 (E_0 = −1.92 V vs. SHE), which is slightly endergonic (ΔG = +2.8 kcal/mol). Among the explored pathways, this reduction step was identified as the most thermodynamically favorable, consistent with prior observations in analogous iron-porphyrin systems for photochemical CO_2-to-CH_4 conversion (24).

Subsequently, the reduced Fe center attacks CO_2, forming transition state **$TS_{3\text{-}3CO2}$** (imaginary frequency: −368 cm^{-1}) with an activation barrier of +8.6 kcal/mol. The resulting adduct **3-CO_2** is energetically uphill (ΔG = +5.2 kcal/mol). Protonation of **3-CO_2** to generate the singlet-state intermediate **4** ($[Fe(II)–COOH]^-$) is barrierless, suggesting a potential spin-crossing event during this step—a phenomenon warranting further investigation.

Following intermediate **4**, protonation of the hydroxyl group by **H_2CO_3** (via transition state **TS4-5**) leads to the formation of **5**, accompanied by the release of an **H_2O molecule**. Both **TS4-5** and intermediate **5** adopt a **singlet ground state**, with the calculated energy barrier for this step being **10.1 kcal/mol**. In intermediate **5**, the **Fe–C** and **C-O** bond distances are **1.71 Å** and **1.15 Å**, respectively. Subsequent one-electron reduction of **5** yields the **(Fe–CO^-)** complex **6**, with a computed redox potential of −1.67 V. At this stage, two divergent pathways emerge: either **CO**

dissociation and **catalyst regeneration**, reforming the active species **2**, or further conversion of **6** into the Fe-methylidene intermediate **13**, as detailed in the catalytic cycle depicted in **Fig. 3b**.

The conversion of **(Fe–CO⁻)** complex **6** to **Fe-methylidene** intermediate **13** is a $3e^-/4H^+$ process that involves a series of elementary reactions. In Fig.3b, the most profitable pathway is illustrated in detail.

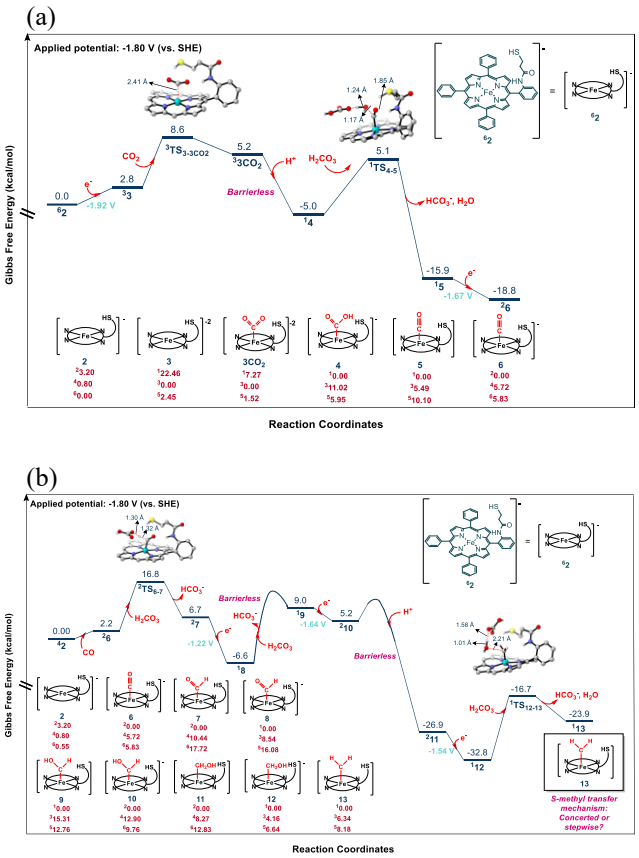

Figure 3. (a) Gibbs free energy diagram (kcal/mol) for the reduction of CO_2 to CO using the active catalyst, complex **2**. **(b)** Gibbs free energy diagram (kcal/mol) for the reduction of (Fe-CO^-) intermediate **6** to Fe-methylidene intermediate **13**.

As shown in Fig.3b, two steps are critical to S-methyl transfer process in this first CO_2 reduction cycle. First, is the protonation of complex **6** to generate the intermediate **7** (Fe-COH). Second, is the final elementary reaction to generate the **Fe-methylidene** intermediate **13**, with the release of one water molecule. In all steps illustrated in Fig.3b, the low-spin intermediate was found to be the ground state with a notably difference in the relative energy between the low-spin state and the other two spin states analyzed.

IRI analysis for the transition state of S-methyl transfer step

After elucidating the catalytic cycle leading to the Fe-methylidene intermediate **13**, we- investigated in detail the *S*-methyl transfer mechanism—a critical step for generating **FeTPPC2SCH3**, the active species responsible for the second CO_2 reduction and subsequent C–C coupling. The transition state for this step is shown below.

Notably, while recent work by Rogge *et al.* demonstrated that Fe-porphyrins mediate cyclopropanation reactions via a *stepwise* triplet-state pathway (involving Fe-methylidene attack by an olefin) (25), our study reveals a distinct *concerted yet asynchronous* C–S insertion for the *S*-methyl transfer. In this mechanism, the H atom is partially transferred to the methylidene prior to sulfur attack, consistent with observations by Fasan *et al.* for *C–C* insertion in iron-porphyrin systems (26). Strikingly, both studies identify the *singlet state* as the energetically preferred pathway, underscoring the generality of this spin-state selectivity in Fe-porphyrin-catalyzed insertion reactions.

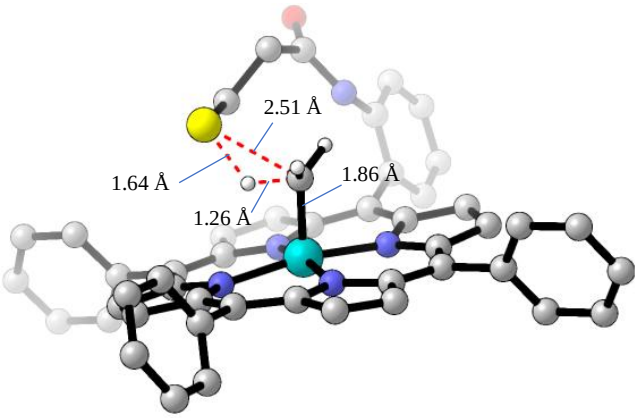

Figure 4. Optimized structure of TS for the S-methyl transfer step. For clarity, all unimportant hydrogen atoms are not shown.

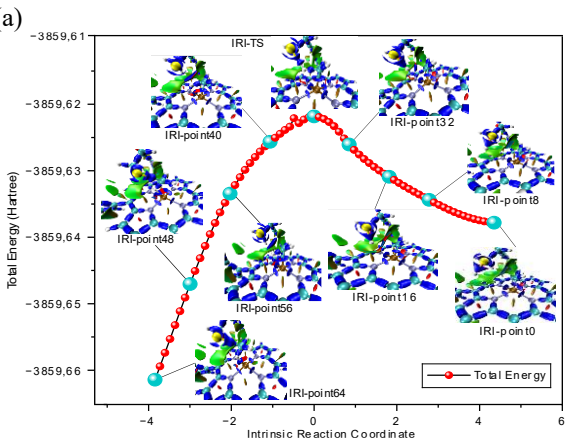

(b)

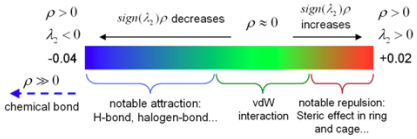

Figure 5. (a) IRC plot for the S-methyl transfer transition state and isosurfaces for key-steps into the IRC coordinate. (b) Standard coloring method and chemical explanation of sign(λ2)ρ on IRI isosurfaces.

To elucidate the nature of the C–S interaction during the *S*-methyl transfer process, we performed an Interaction Region Indicator (IRI) analysis (Fig. 5). The results reveal an early transition state for the C–S insertion, characterized by the absence of strong bonding interactions between the carbon and sulfur atoms, as evidenced by the lack of a critical point in the transition state isosurface.

With the first step of the mechanism now established, the next challenge is to elucidate the pathway for the second CO_2 reduction and subsequent C–C coupling between the two –CH_3 groups, where **FeTPPC$_2$SCH$_3$** serves as the active catalyst for this subsequent catalytic cycle.

Conclusions

The initial step of CO_2 reduction catalyzed by a bioinspired methyltransferase-like iron complex has been successfully modeled computationally, revealing detailed mechanistic insights into both the first CO_2 reduction and the subsequent intramolecular C–S insertion during the *S*-methyl transfer step. The C–S insertion proceeds via a *concerted yet asynchronous* pathway, with the singlet state identified as energetically favored over the triplet state.

Building on these findings, the next critical challenge is to elucidate the mechanism of the *second CO_2 reduction* and the subsequent *C–C coupling* between the two –CH_3 groups incorporated into the catalyst framework, which will complete the catalytic cycle for ethane formation.

Acknowledgements

The authors, are indebted to the financial support from FAPESP, Proc. 2024/15049-0. We are grateful to CNPq and CAPES as well. We are grateful to financial support from Fapesp Proc. 2019/17874-0 and the Center for Computing in Engineering and Sciences at Unicamp (Fapesp Proc. 2013/08293-7).

References

1. C. G. Margarit; C. Schnedermann; N. G. Asimow; D. G. Nocera, *Organometallics* **2019**, *38*, 1219-1223.
2. I. Azcarate; C. Costentin; M. Robert; J.-M. Savéant, *J. Am. Chem. Soc.* **2016**, *138*, 16639-16644.
3. D. J. Martin; J. M. Mayer, *J. Am. Chem. Soc.* **2021**, *143*, 11423-11434.
4. C. A. Obasanjo et al., *Nat. Commun.* **2023**, *14*, 3176.
5. S. Amanullah; P. Saha; A. Dey, *J. Am. Chem. Soc.* **2021**, *143*, 13579-13592.
6. C. G. Margarit; N. G. Asimow; C. Costentin; D. G. Nocera, *ACS Energy Lett.* **2020**, *5*, 72-78.
7. S. Patra; S. Bhunia; S. Ghosh; A. Dey, *ACS Catal.* **2024**, *14*, 7299-7307.
8. S. Patra; S. Dinda; S. Ghosh; T. Roy; A. Dey, *Proc. Natl. Acad. Sci. USA* **2025**, *122*, e2417764122.
9. M. J. Frisch et al., Gaussian 16 Rev. C.01, **2016** (manual técnico)
10. A. D. Becke, *J. Chem. Phys.* **1993**, *98*, 5648-5652.
11. S. Grimme; J. Antony; S. Ehrlich; H. Krieg, *J. Chem. Phys.* **2010**, *132*, 154104-154119.
12. F. Weigend; R. Ahlrichs, *Phys. Chem. Chem. Phys.* **2005**, *7*, 3297-3305.
13. K. Fukui, *J. Phys. Chem. B* **1970**, *74*, 4161-4163.
14. K. Fukui, *Acc. Chem. Res.* **1981**, *14*, 363-368.
15. F. Weigend, *Phys. Chem. Chem. Phys.* **2006**, *8*, 1057-1065.
16. A. V. Marenich et al., *Phys. Chem. Chem. Phys.* **2014**, *16*, 15068-15106.
17. J. Römelt et al., *Inorg. Chem.* **2017**, *56*, 4745-4750.
18. H. Cove; D. Toroz; D. D. Tommaso, *Mol. Catal.* **2020**, *498*, 111248.
19. Y. Wang; W. Lai, *Mol. Catal.* **2024**, *566*, 114430.
20. M. Moura De Salles Pupo; R. Kortlever, *ChemPhysChem* **2019**, *20*, 2926-2935.
21. T. Lu; Q. Chen, *ChemRxiv* **2021**, *1*, 231-239.
22. T. Lu; F. Chen, *J. Comput. Chem.* **2012**, *33*, 580-592.
23. W. Humphrey; A. Dalke; K. Schulten, *J. Mol. Graphics* **1996**, *14*, 33-38.
24. J.-Y. Chen; M. Li; R.-Z. Liao, *Inorg. Chem.* **2023**, *62*, 9400-9417.
25. D. Nam et al., *Nat. Commun.* **2023**, *14*, 7985.
26. T. Rogge et al., *J. Am. Chem. Soc.* **2024**, *146*, 2959-2966.